Progress In Electromagnetics Research, Vol. 164, 63–74, 2019

Efficient Broadband Evaluations of Lattice Green's Functions via Imaginary Wavenumber Components Extractions

Shurun Tan[1, 2, 3, *] and Leung Tsang[3]

Abstract—A novel and systematic method is developed to evaluate periodic Green's functions on empty lattices through extractions of an imaginary wavenumber component of the lattice Green's function and its associated derivatives. We consider cases of volumetric periodicity where the dimensionality of the periodicity has the same dimensionality as the physical problem. This includes one-dimensional (1D) problem with 1D periodicity, two-dimensional (2D) problem with 2D periodicity, and three-dimensional (3D) problem with 3D periodicity, respectively. The remainder of the Green's function is put in spectral series with high-order power-law convergence rates, while the extracted imaginary wavenumber parts are put in spatial series with super-fast and close-to exponential convergence rate. The formulation is free of transcendental functions and thus simple in implementation. It is especially efficient for broadband evaluations of the Green's function as the spatial series are defined on fixed wavenumbers that take small CPU to compute, and the spectral series have simple and separable wavenumber dependences. Keeping only a few terms in both the spatial and spectral series, results of the lattice Green's function are in good agreement with benchmark solutions in 1D, 2D, and 3D, respectively, demonstrating the high accuracy and computational efficiency of the proposed method. The proposed method can be readily generalized to deal with Green's functions including arbitrary periodic scatterers.

1. INTRODUCTION

Volumetric periodic problems are that the dimensionality of the periodicity has the same dimensionality as the physical problem. This includes one-dimensional (1D) problem with 1D periodicity (1D1D), two-dimensional (2D) problem with 2D periodicity (2D2D), and three-dimensional (3D) problem with 3D periodicity (3D3D), respectively. The volumetric periodic Green's function in an empty lattice, also known as the lattice Green's function, denoted by $g_P^0(k, \overline{k}_i; \overline{r}, \overline{r}\,')$, is the field response arising from infinite periodic sources with progressive phase shift $\exp(i\overline{k}_i \cdot \overline{R})$ controlled by the Bloch wave vector $\overline{k}_i$,

$$g_P^0\left(k, \overline{k}_i; \overline{r}, \overline{r}\,'\right) = \sum_{\overline{R}} g^0\left(k; \overline{r}, \overline{r}\,' + \overline{R}\right) \exp\left(i\overline{k}_i \cdot \overline{R}\right) \tag{1}$$

$$= \sum_{\overline{R}} \frac{\exp\left(ik\left|\overline{r} - \left(\overline{r}\,' + \overline{R}\right)\right|\right)}{4\pi\left|\overline{r} - \left(\overline{r}\,' + \overline{R}\right)\right|} \exp\left(i\overline{k}_i \cdot \overline{R}\right) \tag{2}$$

where $\overline{R} = m\overline{a}_1 + n\overline{a}_2 + l\overline{a}_3$, with m, n, l being integer lattice indices and $\overline{a}_1$, $\overline{a}_2$, $\overline{a}_3$ the primary lattice vectors. $g^0(k; \overline{r}, \overline{r}\,')$ is the free-space Green's function at wavenumber k, evaluated at field location $\overline{r}$ and source point $\overline{r}\,'$. In the equation above, the summation over $\sum_{\overline{R}}$ is over three dimensional (3D) lattice.

Received 20 October 2018, Accepted 4 January 2019, Scheduled 28 January 2019

* Corresponding author: Shurun Tan (srtan@umich.edu).

[1] Zhejiang University/University of Illinois at Urbana-Champaign (ZJU-UIUC) Institute, Haining 314400, China. [2] College of Information Science and Electronic Engineering, Zhejiang University, Hangzhou 310027, China. [3] Radiation Laboratory, Department of Electrical and Computer Science, University of Michigan, Ann Arbor, MI 48109-2122, USA.

The points $\overline{r}$ and $\overline{r}'$ are in 3D space. This is the case of volumetric periodic Green's function when the spatial dimension of the physical problem is the same as the dimension of the periodicity. In 3D, $g^0(k;\overline{r},\overline{r}') = \exp(ik|\overline{r}-(\overline{r}'+\overline{R})|)/(4\pi|\overline{r}-\overline{r}'|)$ is the free space Green's function. As indicated in Eq. (1), each of the point source contributes one free-space Green's function component $g^0(k;\overline{r},\overline{r}'+\overline{R})\exp(i\overline{k}_i\cdot\overline{R})$ into $g_P^0(k,\overline{k}_i;\overline{r},\overline{r}')$.

The lattice Green's function, g_P^0, is of special interest to understanding multiple scattering phenomena in periodic structures. It is used widely to formulate integral equations on infinite periodic scatterers while reducing the integral domain to be on a single reference scatterer. Such integral equations lead to band structures and band solutions of periodic structures. Typical periodic structures occur in problems of electromagnetic waves, acoustic waves, and electron waves. Examples include metamaterials [1–3], photonic crystals [4], phononic crystals [5], and atomic crystals [6], etc.

The evaluation of the lattice Green's function g_P^0 is challenging, as it typically involves summing over slowly convergent series, as indicated in Eq. (1), where the spatial series $g^0(k;\overline{r},\overline{r}'+\overline{R})$ decays slowly with distance. In parallel to Eq. (1), the lattice Green's function g_P^0 can also be put into spectral series making use of Poisson summation and the spectral integral representation of g^0,

$$g_P^0\left(k,\overline{k}_i;\overline{r},\overline{r}'\right) = \frac{1}{\Omega}\sum_{\overline{K}}\frac{\exp\left(i\overline{K}\cdot(\overline{r}-\overline{r}')\right)}{\left|\overline{K}\right|^2-k^2} \tag{3}$$

where $\overline{K} = \overline{k}_i + \overline{G}$, and $\overline{G} = m\overline{b}_1 + n\overline{b}_2 + l\overline{b}_3$, with m, n, l being integer reciprocal lattice indices and $\overline{b}_1$, $\overline{b}_2$, $\overline{b}_3$ the reciprocal lattice vectors. The primary and reciprocal lattice vectors satisfy $\overline{a}_i\cdot\overline{b}_j = 2\pi\delta_{ij}$, where δ_{ij} is the Kronecker delta, and $\Omega = (\overline{a}_1\times\overline{a}_2)\cdot\overline{a}_3$ represents the unit cell size. Note that each term in Eq. (3) represents a Floquet plane wave $\exp(i\overline{K}\cdot(\overline{r}-\overline{r}'))$, and it is independent of the wavenumber k. Thus the wavenumber dependence in Eq. (3) is entirely embedded in the rational factor $1/(|\overline{K}|^2-k^2)$, which is much simpler than in $g^0(k;\overline{r},\overline{r}'+\overline{R})$ as in the spatial series in Eq. (1). The summation in Eq. (3) also converges slowly especially when $\overline{r}$ approaches $\overline{r}'$ since $g_P^0(k,\overline{k}_i;\overline{r},\overline{r}')$ is singular at $\overline{r}=\overline{r}'$.

Extensive efforts have been devoted to developing effective techniques to evaluate g_P^0 efficiently. For one-dimensional problem with one-dimensional periodicity, g_P^0, (1D1D), when put in spatial series, can be readily converted into a geometric series and computed [7]. On the other hand, g_P^0 of two-dimensional problem with two-dimensional periodicity (2D2D) [8, 9] and g_P^0 of three-dimensional problem with three-dimensional periodicity (3D3D) [10, 11], in general, are deemed difficult. Ewald's approach [8, 10, 11] is frequently used to decompose the Green's function into a spatial series and a spectral series, both with exponential decay rate. In the Ewald summation [12–15], the decomposition is achieved through judiciously choosing a splitting factor E in a special integral transformation, and the coefficients of the spatial and/or the spectral series involve transcendental functions such as error functions. The formulation of Ewald's approach and its implementation require significant efforts. The wavenumber dependence in Ewald's formulation is in general complicated.

We recently developed the technique of broadband Green's function with low wavenumber extraction (BBGFL) [7, 9, 16–18] to represent the lattice Green's function, and then use it to formulate surface integral equations (SIE) and succeedingly convert the SIE into a linear eigenvalue problem that characterizes the band diagram and the band field solution of the periodic structure. The key concept of BBGFL is to put Eq. (3) into

$$g_P^0\left(k,\overline{k}_i;\overline{r},\overline{r}'\right) = g_P^0\left(k_L,\overline{k}_i;\overline{r},\overline{r}'\right) + \frac{k^2-k_L^2}{\Omega}\sum_{\overline{K}}\frac{\exp\left(i\overline{K}\cdot(\overline{r}-\overline{r}')\right)}{\left(\left|\overline{K}\right|^2-k^2\right)\left(\left|\overline{K}\right|^2-k_L^2\right)} \tag{4}$$

through subtraction of a low wavenumber component $g_P^0(k_L,\overline{k}_i;\overline{r},\overline{r}')$, while improving the convergence rate of the spectral series. In Eq. (4), k_L is chosen as a small (relative to k) and fixed real number that avoids $|\overline{K}|$, and $g_P^0(k_L,\overline{k}_i;\overline{r},\overline{r}')$ is computed through special techniques [7, 9, 17] such as Ewald's summation. The simple wavenumber dependence in Eq. (4) helps in converting the SIE, discretized with the method of moments (MoM), into a linear eigenvalue problem for 1D [7] and 2D [9, 17] photonic crystals, and the fast convergence rate in Eq. (4) significantly reduces the dimension of the resulting eigenvalue problem compared to widely used plane wave expansion method [4, 19]. An overarching

advantage of the BBGFL approach is the ability to accurately construct the band field distribution using relatively few number of plane waves and to effectively normalize the band field distribution without going through tedious volumetric integrals [7, 18]. Such derived band eigenvalues and eigen field solutions are then used to derive Green's function of the periodic structure including scatterers, both due to periodic sources and due to point sources [7, 18]. It is noteworthy that the expansion in the above also applies to Green's function with scatterers. In such a case, the plane wave expansions are replaced by the band field solutions. Low wavenumber extractions are also applied to accelerate the convergence of the band field solutions. The Green's function including periodic scatterers is a key physical quantity in periodic structures and can be used to effectively deal with scattering from bounded periodic scatterers [20] and periodic structure with localized defects [21].

The choice of a real k_L in Eq. (4) renders BBGFL as dependent upon conventional g_P^0 techniques that requires extra work in implementing the method, and choosing a uniform k_L across the entire Brillouin zone is barely feasible to avoid poles in the factor $1/(|\overline{K}|^2 - k_L^2)$. The choice of a uniform k_L over the entire Brillouin zone avoiding band poles is deemed more important in computing the single point source Green's function including periodic scatterers [7, 18], while it is not always feasible to identify a real stop band for a given structure.

In this paper, we deal with these issues by choosing an imaginary wavenumber k_L in Eq. (4),

$$k_L = i\xi \tag{5}$$

where ξ a real number, leading to Eq. (6), to be presented in Section 2.1. This seemingly simple change is innovative. By choosing an imaginary k_L, the spatial representation of $g_P^0(i\xi, \overline{k}_i; \overline{r}, \overline{r}\,')$, as presented in Eq. (7), becomes fast convergent because each term in the spatial summation decays exponentially with separation at an imaginary wavenumber. An imaginary k_L also successfully avoids poles in $1/(|\overline{K}|^2 - k_L^2) = 1/(|\overline{K}|^2 + \xi^2)$ in the entire Brillouin zone. Thus, a self-consistent broadband Green's function technique is formed without seeking help from conventional g_P^0 approaches.

In this paper, we use an imaginary k_L in effectively evaluating g_P^0 over a broadband wavenumber k. The methodologies are illustrated for 1D1D, 2D2D and 3D3D problems, i.e., Green's function with volumetric periodicities. We develop a variety of imaginary wavenumber extraction techniques, leading to high spectral convergence rate of $1/|\overline{K}|^4$, super-high convergence rate of $1/|\overline{K}|^6$, and hyper convergence rate of $1/|\overline{K}|^8$, respectively. The methodology can be readily generalized to even higher order convergence rates of $1/|\overline{K}|^{10}$, $1/|\overline{K}|^{12}$, ..., without substantial complexities. With the hyper convergence rate formulation, we can truncate the spectral series with $|m|$, $|n|$, $|l| \leq 3$, where m, n, l are the lattice indices, to achieve a relative error less than 10^{-3}. The spatial series can be truncated even faster with $|m|$, $|n|$, $|l| \leq 2$ with a relative error less than 10^{-4}. In comparing with Ewald method, the Ewald's method provides exponentially reducing errors and is more favorable in reaching machine accuracies. However, in physical and engineering problems, a relative accuracy of g_P^0 of 10^{-3} is in general sufficient. The proposed method is more efficient than the Ewald approach for this sufficient level of accuracy. It is noteworthy that the proposed acceleration technique through imaginary wavenumber components extractions can also be explained in the general framework of the Kummer's transformation and the Poisson transformation, which has been adopted to accelerate the computation of 3D Green's function with 2D periodicities, i.e., Green's function with surface periodicities [22, 23]. The spectral representation of the Green's function with surface periodicities has exponential decay rate except when the field point approaches the plane of the periodic sources, while the Green's function with volumetric periodicities, in both spectral and spatial representations, converge slowly at all points. Green's function with surface periodicities are for applications in gratings, frequency selective surfaces, etc. Green's functions with volumetric periodicities, the focus of this paper, are for applications in photonic crystals, metamaterials, photonic bandgap (PBG) materials, etc. The use of imaginary wavenumber and imaginary frequencies are used frequently in the study of Casimir forces [24, 25].

The outline of the paper is as follows. In Section 2, we present the formulation, derive the wavenumber derivatives for higher order convergence of the spectral series, and examine the convergence of the spatial series at a single ξ. Numerical results of 1D, 2D and 3D problems are illustrated in Section 3. The conclusions are summarized in Section 4.

2. THE BROADBAND GREEN'S FUNCTION TECHNIQUE USING IMAGINARY WAVENUMBER COMPONENTS EXTRACTIONS

2.1. General Formulation

We verify Eq. (4) by substituting Eq. (3) with $k = k_L$ into Eq. (4) and compare the resulting expression with Eq. (3) at a general k. Now choosing $k_L = i\xi$, i.e., Eq. (5), in Eq. (4), we obtain

$$g_P^0\left(k, \overline{k}_i; \overline{r}, \overline{r}\,'\right) = g_P^0\left(i\xi, \overline{k}_i; \overline{r}, \overline{r}\,'\right) + \frac{\xi^2 + k^2}{\Omega} \sum_{\overline{K}} \frac{\exp\left(i\overline{K} \cdot (\overline{r} - \overline{r}\,')\right)}{\left(\left|\overline{K}\right|^2 - k^2\right)\left(\left|\overline{K}\right|^2 + \xi^2\right)} \tag{6}$$

where $g_P^0(i\xi, \overline{k}_i; \overline{r}, \overline{r}\,')$ is computed from Eq. (1) with $k = i\xi$,

$$g_P^0\left(i\xi, \overline{k}_i; \overline{r}, \overline{r}\,'\right) = \sum_{\overline{R}} g^0\left(i\xi; \overline{r}, \overline{r}\,' + \overline{R}\right) \exp\left(i\overline{k}_i \cdot \overline{R}\right) \tag{7}$$

Note that in Eq. (6), $g_P^0(i\xi, \overline{k}_i; \overline{r}, \overline{r}\,')$ is only required at a fixed ξ, and the Floquet plane waves $\exp(i\overline{K} \cdot (\overline{r} - \overline{r}\,'))$ and the Floquet plane wavevectors $\overline{K}$ are independent of the wavenumber k, leaving the only wavenumber dependence in the rational factor $(\xi^2 + k^2)/(|\overline{K}|^2 - k^2)$. This renders Eq. (6) suitable to be computed over a broadband of wavenumbers. Eq. (6) has a spectral convergence rate of $1/|K^4|$, asymptotically, much improved than the original spectral representation of $g_P^0(k, \overline{k}_i; \overline{r}, \overline{r}\,')$ in Eq. (3) with a spectral convergence rate of $1/|K^2|$. An improved convergence rate implies less Floquet plane waves $\exp(i\overline{K} \cdot (\overline{r} - \overline{r}\,'))$ required in evaluating $g_P^0(k, \overline{k}_i; \overline{r}, \overline{r}\,')$. An additional advantage is that the spectral sum in Eq. (6) is free of singularities at any combination of field points $\overline{r}$ and source points $\overline{r}\,'$, while the spectral poles at $|\overline{K}| = k$ is an intrinsic characteristic of g_P^0. On the other hand, evaluation of $g_P^0(i\xi, \overline{k}_i; \overline{r}, \overline{r}\,')$ through Eq. (7) has exponential convergence rate since $g^0(i\xi; \overline{r}, \overline{r}\,' + \overline{R})$ decays exponentially fast with $|\overline{r} - (\overline{r}' + \overline{R})|$ at $k = i\xi$.

Expressions for g_P^0 with even higher spectral convergence rates are derived through extractions of several wavenumber derivatives at the imaginary wavenumber [20, 26],

$$\begin{aligned} g_P^0\left(k, \overline{k}_i; \overline{r}, \overline{r}\,'\right) \;=\; & g_P^0\left(i\xi, \overline{k}_i; \overline{r}, \overline{r}\,'\right) - \frac{\xi^2 + k^2}{2\xi} \frac{d}{d\xi} g_P^0\left(i\xi, \overline{k}_i; \overline{r}, \overline{r}\,'\right) \\ & + \frac{\left(\xi^2 + k^2\right)^2}{\Omega} \sum_{\overline{K}} \frac{\exp\left(i\overline{K} \cdot (\overline{r} - \overline{r}\,')\right)}{\left(\left|\overline{K}\right|^2 - k^2\right)\left(\left|\overline{K}\right|^2 + \xi^2\right)^2} \end{aligned} \tag{8}$$

and

$$\begin{aligned} g_P^0\left(k, \overline{k}_i; \overline{r}, \overline{r}\,'\right) \;=\; & g_P^0\left(i\xi, \overline{k}_i; \overline{r}, \overline{r}\,'\right) - \frac{\xi^2 + k^2}{2\xi} \frac{d}{d\xi} g_P^0\left(i\xi, \overline{k}_i; \overline{r}, \overline{r}\,'\right) + \frac{\left(\xi^2 + k^2\right)^2}{4\xi} \frac{d}{d\xi}\left[\frac{1}{2\xi} \frac{d}{d\xi} g_P^0\left(i\xi, \overline{k}_i; \overline{r}, \overline{r}\,'\right)\right] \\ & + \frac{\left(\xi^2 + k^2\right)^3}{\Omega} \sum_{\overline{K}} \frac{\exp\left(i\overline{K} \cdot (\overline{r} - \overline{r}\,')\right)}{\left(\left|\overline{K}\right|^2 - k^2\right)\left(\left|\overline{K}\right|^2 + \xi^2\right)^3} \end{aligned} \tag{9}$$

where $\frac{d}{d\xi}$ etc denotes derivatives with respect to wavenumbers. The imaginary wave number components at $k = i\xi$ are computed through spatial series,

$$\frac{d}{d\xi}\left[\frac{1}{\xi} \frac{d}{d\xi} g_P^0\left(i\xi, \overline{k}_i; \overline{r}, \overline{r}\,'\right)\right] = -\frac{1}{\xi^2} \frac{d}{d\xi} g_P^0\left(i\xi, \overline{k}_i; \overline{r}, \overline{r}\,'\right) + \frac{1}{\xi} \frac{d^2}{d\xi^2} g_P^0\left(i\xi, \overline{k}_i; \overline{r}, \overline{r}\,'\right) \tag{10}$$

$$\frac{d}{d\xi} g_P^0\left(i\xi, \overline{k}_i; \overline{r}, \overline{r}\,'\right) = \sum_{\overline{R}} \frac{d}{d\xi} g^0\left(i\xi; \overline{r}, \overline{r}\,' + \overline{R}\right) \exp\left(i\overline{k}_i \cdot \overline{R}\right) \tag{11}$$

$$\frac{d^2}{d\xi^2} g_P^0\left(i\xi, \overline{k}_i; \overline{r}, \overline{r}\,'\right) = \sum_{\overline{R}} \frac{d^2}{d\xi^2} g^0\left(i\xi; \overline{r}, \overline{r}\,' + \overline{R}\right) \exp\left(i\overline{k}_i \cdot \overline{R}\right) \tag{12}$$

One can readily verify Eqs. (6), (8), (9) by substituting

$$g_P^0\left(i\xi,\overline{k}_i;\overline{r},\overline{r}\,'\right)=\frac{1}{\Omega}\sum_{\overline{K}}\frac{\exp\left(i\overline{K}\cdot\left(\overline{r}-\overline{r}\,'\right)\right)}{\left|\overline{K}\right|^2+\xi^2} \tag{13}$$

into each of them and comparing the resulting expressions with Eq. (3), where Eq. (13) is obtained from Eq. (3) with $k=i\xi$.

We note that Eq. (8) and Eq. (9) share the same advantage as Eq. (6), while they enjoy a super-high spectral convergence rate of $1/|\overline{K}|^6$, and a hyper convergence rate of $1/|\overline{K}|^8$, respectively. The number of required Floquet plane waves decreases sharply as we improve the convergence rate of spectral summations. Eqs. (6), (8) and (9) share the same form for lattice Green's function g_P^0 of 1D, 2D, and 3D problems, with an equal dimensionality of periodicities, respectively. It is also noteworthy that in Eqs. (6), (8) and (9) the singularity is only in the first term on the right-hand-side, in $g_P^0(i\xi,\overline{k}_i;\overline{r},\overline{r}\,')$ through Eq. (7) where only a single spatial term $g^0(i\xi;\overline{r},\overline{r}\,'+\overline{R})$ is singular when $\overline{r}$ approaches $\overline{r}\,'+\overline{R}$. Thus, well-developed routines to handle singularities of the free-space Green's function $g^0(i\xi;\overline{r},\overline{r}\,')$ can be directly applied to deal with singularities of $g_P^0(k,\overline{k}_i;\overline{r},\overline{r}\,')$ in integral equations.

2.2. The Free-Space Green's Function and Its Derivatives

In Eqs. (6), (8), (9), we encounter $g_P^0(i\xi,\overline{k}_i;\overline{r},\overline{r}\,')$, $\frac{d}{d\xi}g_P^0(i\xi,\overline{k}_i;\overline{r},\overline{r}\,')$, and $\frac{d^2}{d\xi^2}g_P^0(i\xi,\overline{k}_i;\overline{r},\overline{r}\,')$, which then relates to $g^0(i\xi;\overline{r},\overline{r}\,')$, $\frac{d}{d\xi}g^0(i\xi;\overline{r},\overline{r}\,')$, and $\frac{d^2}{d\xi^2}g^0(i\xi;\overline{r},\overline{r}\,')$, through Eqs. (7), (11), (12), respectively. In this section, we provide the expressions of $g^0(i\xi;\overline{r},\overline{r}\,')$, $\frac{d}{d\xi}g^0(i\xi;\overline{r},\overline{r}\,')$, and $\frac{d^2}{d\xi^2}g^0(i\xi;\overline{r},\overline{r}\,')$, for 1D, 2D, and 3D problems.

2.2.1. 1D Free-Space Green's Function and Its Derivatives

Since

$$g^0\left(k;x,x'\right)=\frac{i}{2k}\exp\left(ik\left|x-x'\right|\right) \tag{14}$$

we have

$$g^0\left(i\xi;x,x'\right)=\frac{1}{2\xi}\exp\left(-\xi\left|x-x'\right|\right) \tag{15}$$

$$\frac{d}{d\xi}g^0\left(i\xi;x,x'\right)=-\left(\frac{1}{\xi}+\left|x-x'\right|\right)g^0\left(i\xi;x,x'\right) \tag{16}$$

$$\frac{d^2}{d\xi^2}g^0\left(i\xi;x,x'\right)=\left[\frac{1}{\xi^2}+\left(\frac{1}{\xi}+\left|x-x'\right|\right)^2\right]g^0\left(i\xi;x,x'\right) \tag{17}$$

Note that there is an exponential decay $\exp(-\xi|x-x'|)$ associated with the imaginary wavenumber. The decay increases sharply with distance between the source and the observation point. Thus, the spatial summation converges fast because the lattice point sources have increasing distances from the observation point.

2.2.2. 2D Free-Space Green's Function and Its Derivatives

Since

$$g^0\left(k;\overline{\rho},\overline{\rho}\,'\right)=\frac{i}{4}H_0^{(1)}\left(k\left|\overline{\rho}-\overline{\rho}\,'\right|\right) \tag{18}$$

we have

$$g^0\left(i\xi;\overline{\rho},\overline{\rho}\,'\right)=\frac{i}{4}H_0^{(1)}\left(i\xi\left|\overline{\rho}-\overline{\rho}\,'\right|\right) \tag{19}$$

$$\frac{d}{d\xi}g^0\left(i\xi;\overline{\rho},\overline{\rho}\,'\right)=\frac{1}{4}\left|\overline{\rho}-\overline{\rho}\,'\right|H_1^{(1)}\left(i\xi\left|\overline{\rho}-\overline{\rho}\,'\right|\right) \tag{20}$$

$$\frac{d^2}{d\xi^2}g^0\left(i\xi;\overline{\rho},\overline{\rho}\,'\right) = \left|\overline{\rho}-\overline{\rho}'\right|^2 g^0\left(i\xi;\overline{\rho},\overline{\rho}\,'\right) - \frac{1}{\xi}\frac{d}{d\xi}g^0\left(i\xi;\overline{\rho},\overline{\rho}\,'\right) \tag{21}$$

where $H_0^{(1)}(\cdot)$ and $H_1^{(1)}(\cdot)$ represent the first kind Hankel function of zeroth and first orders, respectively.

2.2.3. 3D Free-Space Green's Function and Its Derivatives

Since

$$g^0\left(k;\overline{r},\overline{r}\,'\right) = \frac{\exp\left(ik\left|\overline{r}-\overline{r}\,'\right|\right)}{4\pi\left|\overline{r}-\overline{r}\,'\right|} \tag{22}$$

we have, at an imaginary wavenumber,

$$g^0\left(i\xi;\overline{r},\overline{r}\,'\right) = \frac{\exp\left(-\xi\left|\overline{r}-\overline{r}\,'\right|\right)}{4\pi\left|\overline{r}-\overline{r}\,'\right|}$$

then the spatial summation

$$g_P^0\left(i\xi,\overline{k}_i;\overline{r},\overline{r}\,'\right) = \sum_{\overline{R}} \frac{\exp\left(-\xi\left|\overline{r}-\left(\overline{r}\,'+\overline{R}\right)\right|\right)}{4\pi\left|\overline{r}-\left(\overline{r}\,'+\overline{R}\right)\right|}\exp\left(i\overline{k}_i\cdot\overline{R}\right) \tag{23}$$

The convergence is fast as $\overline{R}$ increases with lattice points and the decay with distance at an imaginary wavenumber is exponential. On the other hand, the convergence is poor at a real wavenumber k_L.

Higher order derivatives are

$$\frac{d}{d\xi}g^0\left(i\xi;\overline{r},\overline{r}\,'\right) = -\left|\overline{r}-\overline{r}\,'\right| g^0\left(i\xi;\overline{r},\overline{r}\,'\right) \tag{24}$$

$$\frac{d^2}{d\xi^2}g^0\left(i\xi;\overline{r},\overline{r}\,'\right) = \left|\overline{r}-\overline{r}\,'\right|^2 g^0\left(i\xi;\overline{r},\overline{r}\,'\right) \tag{25}$$

2.3. Error Analysis: Truncating the Spectral and Spatial Series

We examine the criteria to truncate the spectral and spatial series in the hyper convergent formulation, i.e., Eq. (9). These criteria are established to ensure certain level of numerical accuracies in computing g_P^0. It is clear from the following analysis that choosing a larger imaginary wavenumber ξ favors a faster converging spatial series while it slightly decreases the convergence rate of the spatial series. Thus, the choice of ξ is made to balance the number of terms in the spatial and spectral series. In the following analysis, we choose $\xi = \frac{2\pi}{a}$, which successfully truncates both series at $N = 2$ or 3 while achieving high accuracy. Varying ξ slightly around $\frac{2\pi}{a}$ does not alter the performance significantly.

2.3.1. The Spectral Series

The term of interest is

$$\sum_{\overline{K}} \frac{\exp\left(i\overline{K}\cdot\left(\overline{r}-\overline{r}\,'\right)\right)}{\left(\left|\overline{K}\right|^2-k^2\right)\left(\left|\overline{K}\right|^2+\xi^2\right)^3}$$

Let $k = f_n\frac{2\pi}{a}$, where a is the lattice constant and f_n the normalized frequency (or wavenumber), and we assume that $f_n \le 1$ for k of interest, i.e., the lattice constant is equal to or less than the wavenumber. We choose $\xi = \frac{2\pi}{a}$, and let, for a particular $\overline{K} = \overline{k}_i + \overline{G}$, $K = |\overline{K}| = \eta\frac{2\pi}{a}$. Using these definitions, we consider the series at $\overline{r} = \overline{r}\,'$, with worst convergence issues,

$$\sum_{\eta} \frac{1}{\left(\eta^2-f_n^2\right)\left(\eta^2+1\right)^3}$$

For terms of $\overline{K}$ with $\eta \gg 1 \geq f_n$, this asymptotically reduces to $\sum_\eta \frac{1}{\eta^8}$ with η approaching integers. Without significantly changing its convergence properties, we examine the integer series,

$$\sum_n \frac{1}{n^{(8-\mathrm{Dim}+1)}}$$

where Dim = 1, 2, 3, respectively, for 1D, 2D, and 3D problems. The decreasing of the exponent of n as we raise the dimensionality of the problem is due to the increasing occurrences of terms with similar amplitudes, i.e., the summation $\sum_\eta$ is over a single, double and triple indices for 1D, 2D and 3D problems, respectively.

Straightforward evaluations show that, to reach a relative error less than 10^{-3}, we need $|n| \leq N$, with $(2N+1)^{\mathrm{Dim}}$ terms in the spectral series,

$$\begin{aligned} N &= 2, \text{ for 1D, } 2N+1 = 5 \\ N &= 2, \text{ for 2D, } (2N+1)^2 = 25 \\ N &= 3, \text{ for 3D, } (2N+1)^3 = 343 \end{aligned}$$

Note that the required number of terms are similar to those required in Ewald summations. However, Ewald summation involves complicated special functions (error functions), and is more computationally expensive than the proposed approach. In solving integral equations with g_P^0, the matrix elements involve integrations of g_P^0 over a particular region, which in general enjoy better accuracy than g_P^0 due to phase cancelations.

2.3.2. The Spatial Series

We note from Section 2.2 that

$$g^0, \frac{d}{d\xi}g^0, \frac{d^2}{d\xi^2}g^0\left(i\xi;\overline{r},\overline{r}\,'\right) \propto \left|\overline{r}-\overline{r}\,'\right|^\alpha \exp\left(-\xi\left|\overline{r}-\overline{r}\,'\right|\right)$$

with $\alpha \leq 2, 1.5$, and 1, for 1D, 2D, and 3D problems, respectively. Thus, all these terms have close to exponential decay rates with respect to the distance $|\overline{r}-\overline{r}\,'|$. Thus, the terms of the spatial series, as illustrated in Eqs. (7), (11), (12), share the form, asymptotically,

$$\left|\overline{r}-\overline{r}\,'-\overline{R}\right|^\alpha \exp\left(-\xi\left|\overline{r}-\overline{r}\,'-\overline{R}\right|\right)\exp\left(i\overline{k}_i\cdot\overline{R}\right).$$

Choosing $\xi = \frac{2\pi}{a}$ and letting $|\overline{r}-\overline{r}\,'-\overline{R}| = \zeta a$, this becomes

$$\zeta^\alpha a^\alpha \exp\left(-2\pi\zeta\right)\exp\left(i\overline{k}_i\cdot\overline{R}\right)$$

We eliminate the phase factor and consider the convergence rate of an integer series,

$$\sum_n n^{\alpha+(\mathrm{Dim}-1)}\exp\left(-2\pi n\right)$$

where the factor $n^{\mathrm{Dim}-1}$ again arises from the increasing dimension of summation indices and Dim = $1, 2, 3$ represents the dimensionality of periodicity, for 1D, 2D, and 3D problems, respectively. Truncating the summation with $|n| \leq N$ leads to $(2N+1)^{\mathrm{Dim}}$ terms in the series.

Simple calculations show that truncating the series with $N = 2$ leads to relative error less than 10^{-4}, and truncating with $N = 3$ leads to relative error less than 10^{-6}. Thus $N = 2$ is in general accurate enough in truncating the spatial series.

2.4. Bloch Condition of g_P^0

g_P^0 satisfies the Bloch wave conditions,

$$g_P^0\left(k,\overline{k}_i;\overline{r}+\overline{R},\overline{r}\,'\right) = g_P^0\left(k,\overline{k}_i;\overline{r},\overline{r}\,'\right)\exp\left(i\overline{k}_i\cdot\overline{R}\right) \tag{26}$$

thus for arbitrary $\overline{r}$ and $\overline{r}'$, we can find a vector $\overline{r}_0$, with its length $r_0 = |\overline{r}_0| \leq \frac{a}{2}$, through

$$\overline{r}-\overline{r}\,' = \overline{r}_0 + \overline{R}$$

then

$$g_P^0\left(k,\overline{k}_i;\overline{r}-\overline{r}\,'\right)=g_P^0\left(k,\overline{k}_i;\overline{r}_0\right)\exp\left(i\overline{k}_i\cdot\overline{R}\right) \tag{27}$$

We thus compute $g_P^0(k,\overline{k}_i;\overline{r}_0)$ with Eqs. (6), (8), (9), and then obtain $g_P^0(k,\overline{k}_i;\overline{r}-\overline{r}\,')$ through Eq. (27) applying the multiplicative phase factor $\exp(i\overline{k}_i\cdot\overline{R})$. It is much more regularized to compute $g_P^0(i\xi,\overline{k}_i;\overline{r}_0)$ than computing $g_P^0(i\xi,\overline{k}_i;\overline{r}-\overline{r}\,')$ using the spatial series.

3. NUMERICAL RESULTS AND DISCUSSIONS

In this section, we apply the proposed formulation of Eq. (9) to 1D, 2D, and 3D problems with volumetric periodicity. We illustrate its high efficiency and accuracy through comparisons with benchmark solutions in [7, 9, 17], and [11], for 1D, 2D, and 3D problems, respectively.

In all the numerical examples to be reported, we choose $\xi = 2\pi/a$, with a being the lattice constant. We uniformly truncate the spatial series up to $N_{\text{spa}} = 2$, and we truncate the spectral series up to $N_{\text{spe}} = 2, 2, 3$, for 1D, 2D, and 3D problems, respectively. We define $k = f_n\frac{2\pi}{a}$ with f_n being the normalized wavenumber (or frequency). We use "BBGFL" in the figure illustrations to denote the proposed method.

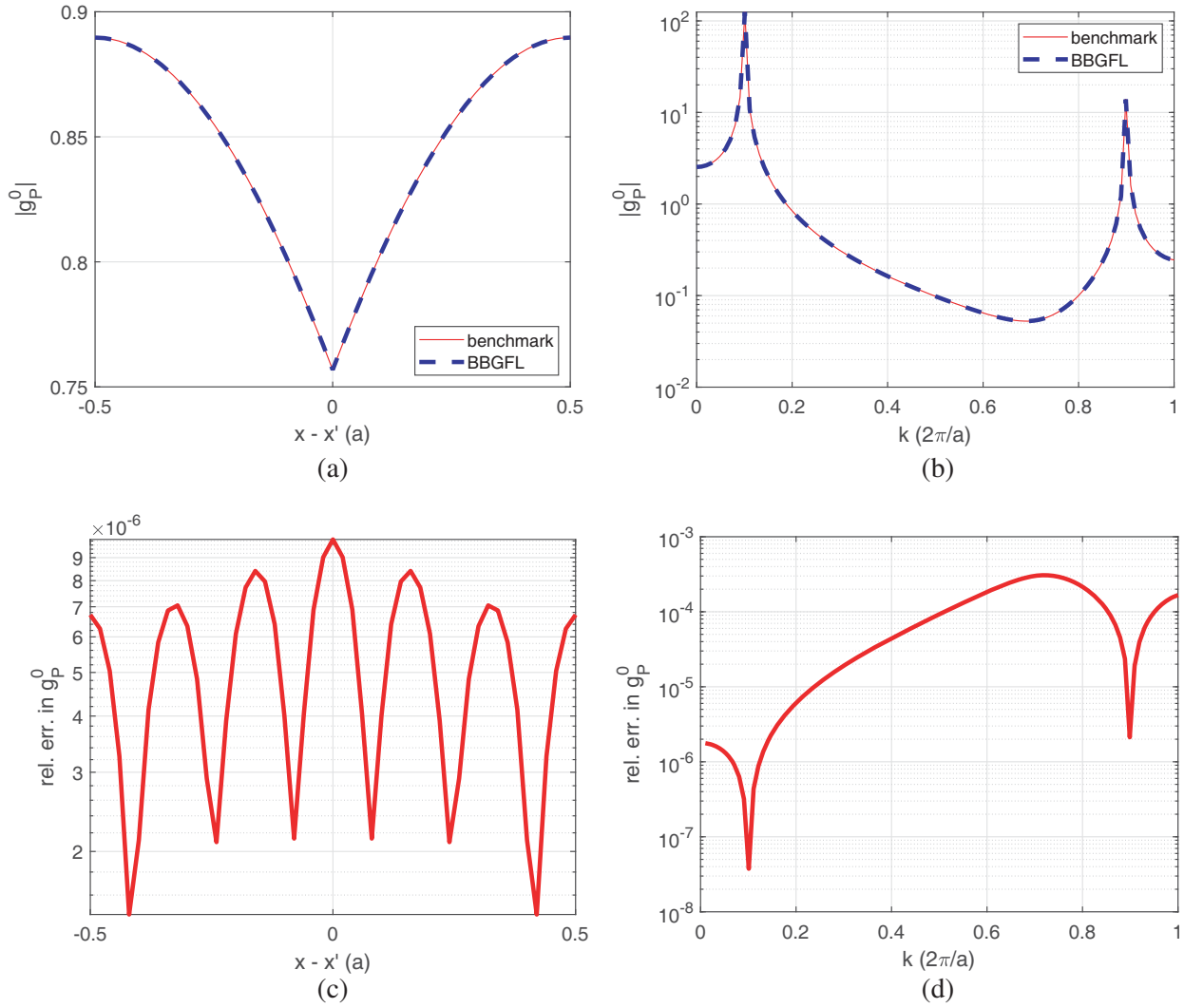

Figure 1. g_P^0 of 1D problem with 1D periodicity. The benchmark solutions are computed according to [7]. "BBGFL" represents the proposed method following Eq. (9). (a) g_P^0 vs. $x-x'$, $f_n = 0.2$, (b) g_P^0 vs. k, $x-x' = 0.2a$, (c) relative error vs. $x-x'$, $f_n = 0.2$, (d) relative error vs. k, $x-x' = 0.2a$.

3.1. 1D Problem with 1D Periodicity

Let $k_i = \beta\frac{2\pi}{a}$ and $\beta = 0.1$. In Fig. 1(a) and Fig. 1(c), we plot $g_P^0(k, \overline{k}_i; x, x')$ and its relative error as a function of the separation $x - x'$, respectively, where we have chosen $f_n = 0.2$, and $-a/2 < x - x' < a/2$. In Fig. 1(b) and Fig. 1(d), we plot $g_P^0(k, \overline{k}_i; x, x')$ and its relative error as a function of the wavenumber k, respectively, where we have chosen $x - x' = 0.2a$, and $0 \leq f_n \leq 1$.

3.2. 2D Problem with 2D Periodicity

We use a square lattice to illustrate results with primary lattice vectors $\overline{a}_1 = a\widehat{x}$, $a_2 = a\widehat{y}$, and reciprocal lattice vectors $\overline{b}_1 = \frac{2\pi}{a}\widehat{x}$, $\overline{b}_2 = \frac{2\pi}{a}\widehat{y}$. Let $\overline{k}_i = \beta_1\overline{b}_1 + \beta_2\overline{b}_2$, and $\beta_1 = 0.1$, $\beta_2 = 0$. In Fig. 2(a) and Fig. 2(c), we plot $g_P^0(k, \overline{k}_i; \overline{\rho}, \overline{\rho}')$ and its relative error as a function of $\overline{\rho} - \overline{\rho}'$, respectively, where we have chosen $f_n = 0.2$, $\overline{\rho} - \overline{\rho}' = (x - x')\widehat{x}$ and $-a/2 < x - x' < a/2$. In Fig. 2(b) and Fig. 2(d), we plot $g_P^0(k, \overline{k}_i; \overline{\rho}, \overline{\rho}')$ and its relative error as a function of the wavenumber k, respectively, where we have chosen $\overline{\rho} - \overline{\rho}' = 0.2a\widehat{x}$ and $0 \leq f_n \leq 1$.

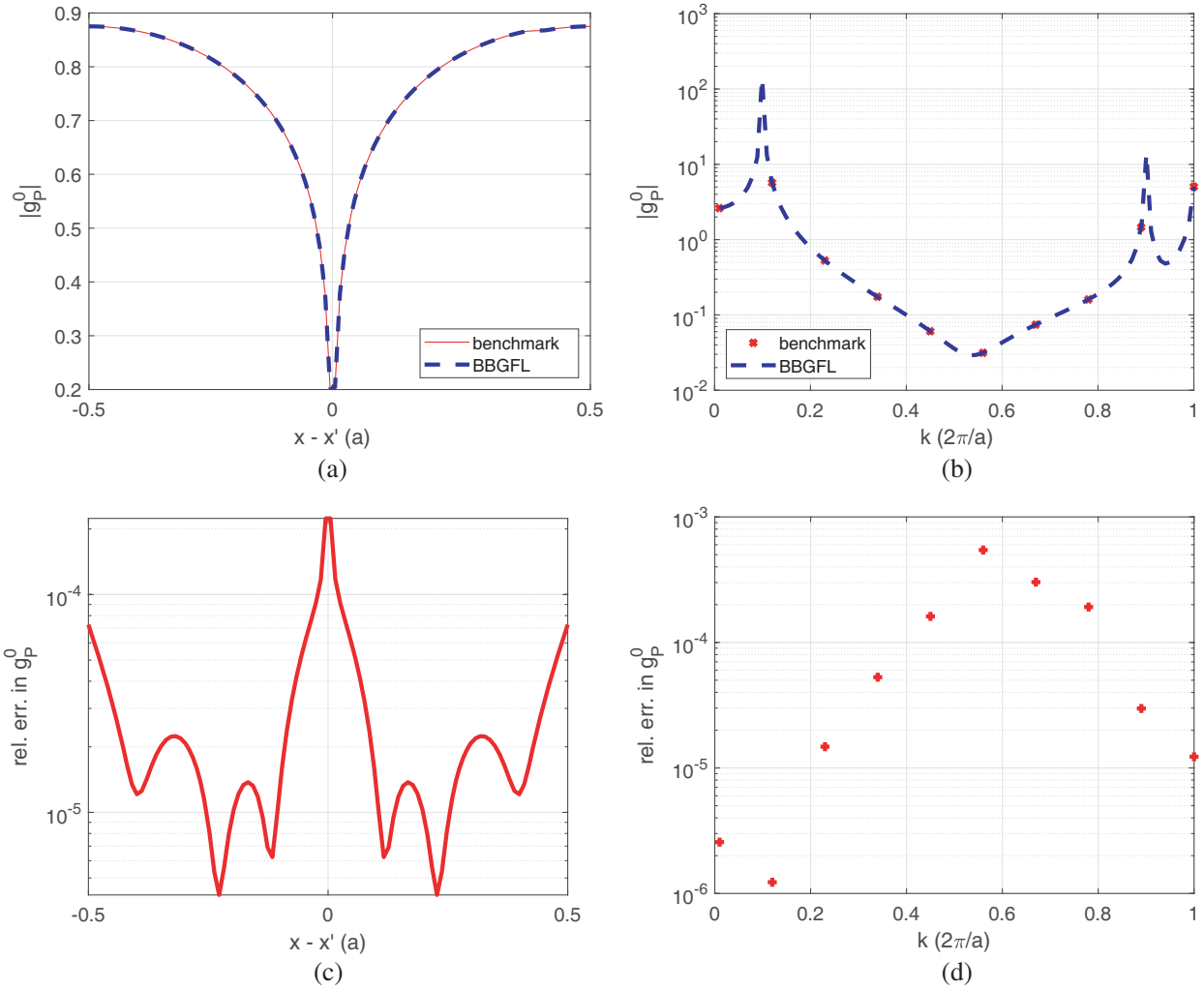

Figure 2. g_P^0 of 2D problem with 2D periodicity. The benchmark solutions are computed according to [9, 17]. "BBGFL" represents the proposed method following Eq. (9). (a) g_P^0 vs. $x - x'$, $f_n = 0.2$, (b) g_P^0 vs. k, $x - x' = 0.2a$, (c) relative error vs. $x - x'$, $f_n = 0.2$, (d) relative error vs. k, $x - x' = 0.2a$.

3.3. 3D Problem with 3D Periodicity

We use a cubic lattice to illustrate results with primary lattice vectors $\overline{a}_1 = a\widehat{x}$, $a_2 = a\widehat{y}$, $a_3 = a\widehat{z}$ and reciprocal lattice vectors $\overline{b}_1 = \frac{2\pi}{a}\widehat{x}$, $\overline{b}_2 = \frac{2\pi}{a}\widehat{y}$, $\overline{b}_3 = \frac{2\pi}{a}\widehat{z}$. Let $\overline{k}_i = \beta_1\overline{b}_1 + \beta_2\overline{b}_2 + \beta_3\overline{b}_3$, and $\beta_1 = 0.1$, $\beta_2 = 0$, $\beta_3 = 0$. In Fig. 3(a) and Fig. 3(c), we plot $g_P^0(k, \overline{k}_i; \overline{r}, \overline{r}\,')$ and its relative error as a function of $\overline{r} - \overline{r}\,'$, respectively, where we have chosen $f_n = 0.2$, $\overline{r} - \overline{r}\,' = (x - x')\widehat{x}$ and $-a/2 < x - x' < a/2$. In Fig. 3(b) and Fig. 3(d), we plot $g_P^0(k, \overline{k}_i; \overline{r}, \overline{r}\,')$ and its relative error as a function of the wavenumber k, respectively, where we have chosen $\overline{r} - \overline{r}\,' = 0.2a\widehat{x}$ and $0 \le f_n \le 1$.

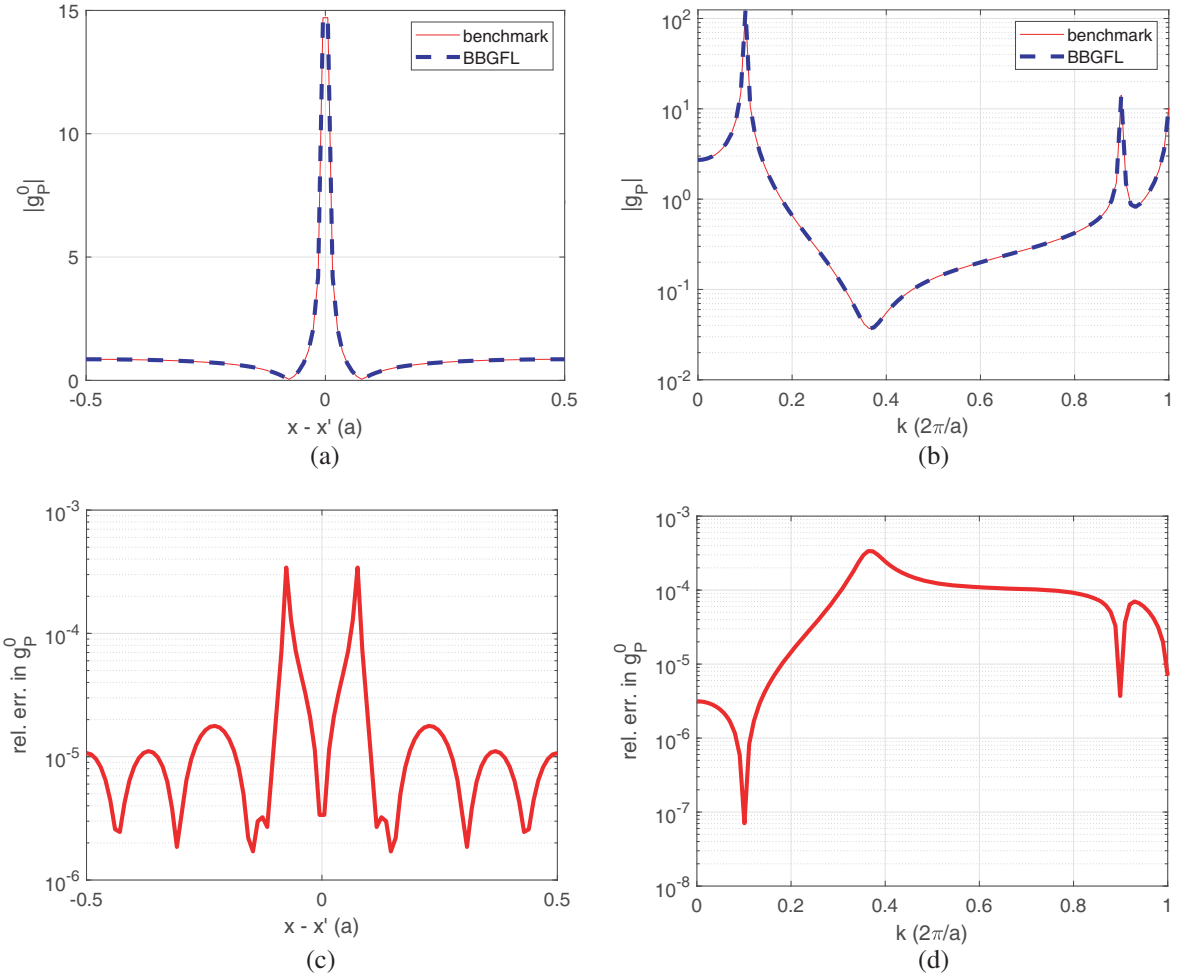

Figure 3. g_P^0 of 3D problem with 3D periodicity. The benchmark solutions are computed according to [11]. "BBGFL" represents the proposed method following Eq. (9). (a) g_P^0 vs. $x - x'$, $f_n = 0.2$, (b) g_P^0 vs. k, $x - x' = 0.2a$, (c) relative error vs. $x - x'$, $f_n = 0.2$, (d) relative error vs. k, $x - x' = 0.2a$.

The numerical examples have demonstrated high accuracy and efficiency of the proposed method for a broadband wavenumber k and for arbitrary field point/source point separations $\overline{r} - \overline{r}\,'$. Using the formulation with hyper spectral convergence rate of $|\overline{K}|^{-8}$, we readily obtain relative errors less than 10^{-3} by truncating the spatial series at $N_{\text{Spa}} = 2$ for all problem dimensions, and truncating the spectral series at $N_{\text{Spe}} = 2, 2, 3$, for 1D, 2D, and 3D problems, respectively. The results have proved the effectiveness of the error analysis. These criteria are similar to those used in Eward's method truncating the spatial and spectral series. The demonstrated relative errors peak at several points when $g_P^0 \to 0$ which exacerbates the relative errors. Further tests show that the small absolute error uniformly increases with k. Increasing N_{Spe} by 1 reduces the error but not significantly, and it does not change

the overall pattern of the relative error versus k. Developing formulations with even higher spectral convergence rate is possible and straightforward to further reduce numerical errors and can be more efficient than increasing N_{Spe} significantly.

4. CONCLUSIONS

A self-consistent and widely applicable technique is developed to efficiently evaluate the lattice Green's function over a broadband wavenumber with high accuracy through extractions of several imaginary wavenumber components. The extracted components, being effectively evaluated in spatial series at a fixed imaginary wavenumber, have removed the singularity, avoided unnecessary poles, and substantially improved the convergence rate of the remaining spectral series. Unlike conventional techniques that must be developed separately case by case for different dimensionalities invoking special integral transformations, the proposed technique is easy to implement, and it generally applies to lattice Green's functions in 1D1D, 2D2D, and 3D3D problems. Expressions of the scalar lattice Green's function with high spectral convergence rate of K^{-4}, K^{-6}, and K^{-8} are derived and examined, readily extensible to even higher orders. The K^{-8} formulation readily achieves relative errors less than 10^{-3} by truncating the spectral series up to $N = 2$ or 3. A high convergence rate is not only desired to reduce the number of Floquet plane waves or band field solutions that must be included to accurately compute the Green's function, but also necessary to evaluate the dyadic Green's function which is in general associated with a lower convergence rate than its scalar counterpart. The proposed method can be readily generalized to deal with Green's functions including arbitrary periodic scatterers, both arising from periodic sources with a progressive phase shift and from a single point source. There are physical reasons why an imaginary low wavenumber extraction works better than a real low wavenumber extraction. In the real low wavenumber extraction, the extraction accounts for $1/r$ dependence for the near field. However, the $1/r$ dependence extends to long distances and becomes inconvenient for far field. For the imaginary low wavenumber extraction, one has $\exp(-\xi r)/r$ dependence. Because ξ is not large, for near field the extraction is just $1/r$ as in the real low wavenumber extraction. However, for far field the extraction decays exponentially and vanishes. The proposed method achieves uniform convergence in both the spatial and the spectral series for all field/source points of the lattice Green's function. In this paper, we study imaginary wavenumber extractions for periodic Green's function in empty lattice. We are presently applying the imaginary wavenumber extractions to Green's functions, including the effects of scatterers, in volumetric periodic problems. The method can also be generalized to deal with cases where the dimensionality of periodicity is less than the space dimensionality, well representative of gratings and metasurfaces. In this reduced dimensionality of periodicity scenario, e.g., 2D1D, and 3D2D problems, evaluation of the lattice Green's function when both field points and source points are on the same plane parallel to the lattice vectors poses challenges and difficulties to conventional Green's function techniques. Extensions of the proposed imaginary wavenumber extraction technique for these problems are also being studied.

REFERENCES

1. Pendry, J. B., A. J. Holden, D. J. Robbins, and W. J. Stewart, "Low frequency plasmons in thin-wire structures," *J. Phys.: Condens. Matter*, Vol. 10, 4785–4809, 1998.
2. Pendry, J. B., A. J. Holden, D. J. Robbins, and W. J. Stewart, "Magnetism from conductors and enhanced nonlinear phenomena," *IEEE Trans. Microw. Theory Techn.*, Vol. 47, No. 11, 2075–2084, 1999.
3. Smith, D. R., W. J. Padilla, D. C. Vier, S. C. Nemat-Nasser, and S. Schultz, "Composite medium with simultaneously negative permeability and permittivity," *Phys. Rev. Lett.*, Vol. 84, No. 18, 4184–4187, 2000.
4. Joannopoulos, J. D., S. G. Johnson, J. N. Winn, and R. D. Meade, *Photonic Crystals: Molding the Flow of Light*, Princeton University Press, 2011.
5. Yang, Z., F. Gao, X. Shi, X. Lin, Z. Gao, Y. Chong, and B. Zhang, "Topological acoustics," *Phys. Rev. Lett.*, Vol. 114, No. 11, 114301, 2015.

6. Haldane, F. D. M., "Model for a quantum Hall effect without Landau levels: Condensed-matter realization of the "parity anomaly"," *Phys. Rev. Lett.*, Vol. 61, No. 18, 2015–2018, 1988.
7. Tsang, L., K.-H. Ding, and S. Tan, "Broadband point source Green's function in a one-dimensional infinite periodic lossless medium based on BBGFL with modal method," *Progress In Electromagnetics Research*, Vol. 163, 51–77, 2018.
8. Leung, K. M. and Y. Qiu, "Multiple-scattering calculation of the two-dimensional photonic band structure," *Physical Review B*, Vol. 48, No. 11, 7767–7771, 1993.
9. Tsang, L., "Broadband calculations of band diagrams in periodic structures using the broadband Green's function with low wavenumber extraction (BBGFL)," *Progress In Electromagnetics Research*, Vol. 153, 57–68, 2015.
10. Kohn, W. and N. Rostoker, "Solution of the Schrödinger equation in periodic lattices with an application to metallic lithium," *Physical Review*, Vol. 94, 1111–1120, 1954.
11. Silveirinha, M. and C. A. Fernandes, "A new method with exponential convergence to evaluate the periodic Green's function," *Proc. IEEE APS/URSI Symp.*, Vol. 2, 805–808, Columbus, OH, Jun. 2003.
12. Ewald, P. P., "Die berechnug optischer und elekrostatischen gitterpotential," *Ann. Phys.*, Vol. 64, 253–268, 1921.
13. Jordan, K. E., G. R. Richter, and P. Sheng, "An efficient numericalevaluation of the Green's functionfor the Helmholtzoperator on periodic structures," *J. Comp. Phys.*, Vol. 63, 222–235, 1986.
14. Mathis, A. W. and A. F. Peterson, "A comparisonof acceleration procedures for the two-dimensional periodic Green's function," *IEEE Trans. Antennas Propag.*, Vol. 44, 567–571, Apr. 1996.
15. Tsang, L., J. A. Kong, K.-H. Ding, and C. O. Ao, *Scattering of Electromagnetic Waves, Vol. 2, Numerical Simulations*, Wiley-Interscience, New York, 2001.
16. Tan, S., "Multiple volume scattering in random media and periodic structures with applications in microwave remote sensing and wave functional materials," PhD Thesis, University of Michigan, https://deepblue.lib.umich.edu/handle/2027.42/137141, 2016.
17. Tsang, L. and S. Tan, "Calculations of band diagrams and low frequency dispersion relations of 2D periodic dielectric scatterers using broadband Green's function with low wavenumber extraction (BBGFL)," *Opt. Express*, Vol. 24, 945–965, 2016.
18. Tan, S. and L. Tsang, "Green's functions, including scatterers, for photonic crystals and metamaterials," *J. Opt. Soc. Am. B*, Vol. 34, 1450–1458, 2017.
19. Johnson, S. G. and J. D. Joannopoulos, "Block-iterative frequency-domain methods for Maxwell's equations in a planewave basis," *Opt. Express*, Vol. 8, 173–190, 2001.
20. Tan, S. and L. Tsang, "Scattering of waves by a half-space of periodic scatterers using broadband Green's function," *Opt. Lett.*, Vol. 42, 4667–4670, 2017.
21. Tan, S. and L. Tsang, "Effects of localized defects/sources in a periodic lattice using Green's function of periodic scatterers," *IEEE International Symposium on Antennas and Propagation and USNC-URSI Radio Science Meeting*, Boston, MA, USA, 2018.
22. Singh, S., W. F. Richards, J. R. Zinecker, and D. R. Wilton, "Accelerating the convergence of series representing the free space periodic Green's function," *IEEE Trans. Antennas Propag.*, Vol. 38, No. 12, 1958–1962, 1990.
23. Ivanishin, M. M. and S. P. Skobelev, "A modification of the Kummer's method for efficient computation of the Green's function for doubly periodic structures," *IEEE Trans. Antennas Propag.*, Vol. 57, No. 9, 2794–2798, 2009.
24. Lifshitz, E. M., "The theory of molecular attractive forces between solids," *Soviet Physics*, Vol. 2, No. 1, 73–83, 1956.
25. Simpson, W. M. and U. Leonhardt, *Forces of the Quantum Vacuum: An Introduction to Casimir Physics*, World Scientific Publishing Company, 2015.
26. Tsang, L., K. H. Ding, T. H. Liao, and S. Huang, "Modeling of scattering in arbitrary-shape waveguide using broadband Green's function with higher order low wavenumber extractions," *IEEE Transactions on Electromagnetic Compatibility*, Vol. 60, No. 1, 16–25, Feb. 2018.